High-Resolution Downscaling of Urban Land Surface Temperature via Machine Learning

Naeim Mijani [1], James Voogt [1], Mohammad Karimi Firozjaei [2], Majid Kiavarz [3]

[1] Department of Geography and Environment, Western University, London, ON N6A 5C2, Canada – nmijani@uwo.ca, javoogt@uwo.ca
[2] College of Management, University of Tehran, Tehran, Iran – mohammad.karimi.f@ut.ac.ir
[3] Department of Remote Sensing and GIS, University of Tehran, Tehran, 1417964743, Iran – kiavarzmajid@ut.ac.ir

Keywords: Urban thermal environment, Land surface temperature, Downscaling, Machine learning, Thermal remote sensing.

Abstract

Land surface temperature (LST) obtained from satellite observations is a key parameter for understanding Earth surface-atmosphere energy exchange and urban thermal environments. However, the use of existing satellite-derived LST datasets for urban applications is limited by the coarse spatial resolution and the mixed-pixel problem. By integrating both two-dimensional (2D) surface properties and three-dimensional (3D) urban morphological characteristics, this study proposes a machine learning-based framework for high-resolution downscaling of satellite-based urban land surface temperature (SULST). A Random Forest model was developed to generate a 1-m downscaled SULST (DSULST) map. The model demonstrates strong performance, with a Pearson correlation coefficient of 0.89, RMSE of 1.15 K, NRMSE of 0.095, MAE of 0.56 K, and an index of agreement of 0.95. The 1-m DSULST maps reveal substantial sub-pixel thermal heterogeneity that is not captured by conventional 30-m LST data. Fine-scale spatial patterns associated with vegetation, building structures, and roads are clearly resolved in the downscaled 1-m temperature maps. These results highlight a critical limitation of satellite-derived LST in representing intra-urban thermal variability. The findings demonstrate that enhancing the spatial resolution of urban LST is essential for urban applications, including modeling surface energy fluxes, pedestrian-level heat exposure, and energy consumption, all of which benefit from higher spatial resolution.

1. Introduction

Land surface temperature (LST) is a key component of the urban-modified climate because it represents a solution to the surface energy budget - the inputs and outputs of heat at the surface (Firozjaei et al., 2020; Garuma et al., 2018; Voogt and Oke, 2003). LSTs are critical to urban applications such as thermal comfort, the urban heat island, public health, and energy consumption (Mashhoodi et al., 2020; Mijani et al., 2020; Nuñez et al., 2023; Tanoori et al., 2024). A major issue for urban applications is the coarse spatial resolution and the biased sampling associated with current satellite-derived LST. Satellite-based urban land surface temperature (SULST) for each pixel generally represents the mean temperature of various surface elements, which can introduce significant errors into the results (Firozjaei et al., 2023; Firozjaei et al., 2024). In dense and structurally diverse urban areas, this can lead to SULST representing a mix of surfaces with varying thermal responses (Firozjaei et al., 2022b), such as building roofs, ground surfaces, and tree canopy tops, which may not correspond to the surfaces relevant to specific applications such as pedestrian thermal comfort. In a downscaled image, irrelevant surfaces (e.g., roofs) can be identified and excluded, allowing a better identification of inputs relevant to pedestrian-level heat exposure, such as ground level land surface temperature and shading fractions.

Urban applications require highly accurate and spatially explicit surface temperatures at the micro-urban scale (1-5 m), particularly at the level of individual building blocks, street canyons, and fine urban textures. Such high-resolution data enable a more precise representation of the thermal heterogeneity inherent in urban environments, where temperature distributions are strongly controlled by complex interactions among land cover types, material properties, vegetation presence, and both two-dimensional (2D) and three-dimensional (3D) urban morphological characteristics (Firozjaei et al., 2022a). However, coarse-resolution thermal imagery significantly reduces the reliability of urban LST estimates and limits the ability to detect localized thermal anomalies, such as heat hotspots associated with impervious surfaces or cooling effects related to vegetation and water bodies. Therefore, it is important to develop a new downscaling model that can simultaneously consider the temperature value and its spatial neighborhood relationships.

Current and upcoming thermal datasets continue to have spatial resolutions that are substantially coarser than the scale at which most urban surface temperature variability occurs. Most satellite-based thermal sensors are designed with broader regional or global monitoring objectives, resulting in spatial resolutions that are considerably coarser than what is needed for detailed urban studies. Consequently, these datasets are often insufficient for capturing intra-urban thermal variability and for analyzing the localized impacts of urban form and land surface characteristics.

Airborne platforms, such as helicopters and unmanned aerial vehicles (UAVs), offer a potential solution by providing thermal imagery with very high spatial resolution, sometimes reaching sub-meter levels. Despite this advantage, their application in large-scale or long-term urban studies remains constrained by several practical and economic limitations. These include limited spatial coverage, making it difficult to map entire cities; challenges in conducting repeated and consistent data acquisition over time; sensitivity to weather and operational conditions; and relatively high costs associated with deployment, maintenance, and data processing. These constraints have prevented the widespread adoption of airborne thermal data in routine urban analysis and decision-making processes.

Given these limitations, improving the accuracy and spatial resolution of sub-pixel urban LST estimation has become a critical research priority. This is particularly important in heterogeneous urban landscapes, where significant thermal variability can occur within a single coarse-resolution pixel. Advanced techniques such as thermal sharpening, data fusion,

https://doi.org/10.5194/isprs-archives-XLIX-B3-2026-405-2026

and machine learning-based downscaling have been explored to overcome these challenges (Bahi et al., 2025; Tahooni et al., 2025).

However, existing studies mainly focus on the independent analysis of urban morphological factors, and the relative contributions of integrating 2D and 3D urban morphology characteristics to reconstruct finer-scale temperature patterns remain limited. In complex urban environments, accurately capturing the spatial variability of urban LST in relation to both 2D surface properties (such as albedo, land cover, and vegetation indices) and 3D urban structure (including sky view factor, building height, and density) is essential for a deeper understanding of urban thermal environments.

Such improvements not only enhance the scientific understanding of urban heat dynamics but are also essential for addressing urban environmental challenges characterized by high spatial variability, such as the Urban Heat Island (UHI) phenomenon (Voogt and Oke, 2003). The main objective of this research is the integration of 2D and 3D urban morphological characteristics with advanced machine learning techniques to create urban LST estimates at a 1-m sub-pixel scale to detect the fine-scale variability in surface thermal patterns that are not captured by conventional thermal remote sensing.

2. Study area

The study area is located in the northeastern part of Tehran, Iran. It is situated at approximately 35.75° N and 51.42° E and covers a total area of about 4.44 km2. Fig. 1 shows the study area and its major land use. The study area includes various land cover types such as buildings, barren lands, roads, vegetation, and water bodies, indicating a heterogeneous environment. Building heights range from 3 to 102 meters, reflecting a mix of low- and high-rise structures. Vegetation height varies between 0.2 and 16 meters, representing different types of plant cover from grass to trees. The elevation of the area ranges from 1363 to 1585 meters above sea level, with an average elevation of 1423 meters. The region is characterized by a hot and arid climate. The study area experiences an average relative humidity of approximately 40%, with winds at an average speed of 5.5 m/s, predominantly blowing from the west.

Precipitation varies across the area, with annual totals of about 262 mm in the northern part to 145 mm in the southeastern part of the study area. The area typically has approximately 60 days of rainfall and around 210 clear-sky days per year, which contributes to increased solar radiation and higher surface temperatures.

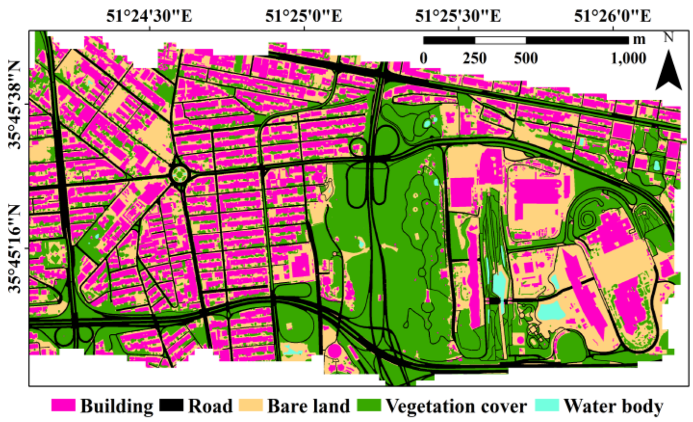

Figure 1. Land use map of the study area showing the spatial distribution of major surface types.

3. Data

The input layers used in this study consist of a set of 2D and 3D urban morphological variables derived from multiple data sources. Specifically, four primary datasets were utilized, including DSM, Landsat 9 surface temperature products, high-resolution Google Earth imagery, and land use maps. The 2D variables include land use/land cover classes (e.g., built-up areas, vegetation, roads) extracted from land use maps and visual interpretation of Google Earth imagery. These variables represent the biophysical properties of the urban surface that influence thermal behavior. The 3D variables were derived from the DSM, capturing the vertical structure of the urban environment such as buildings and terrain variability. These variables were selected as they collectively represent key drivers of urban land surface temperature, including surface material, vegetation presence, and urban geometry.

Nine Landsat 9 satellite images around 10:30 local time (corresponding to the Landsat 9 overpass) during the April-September 2023 period were selected. Urban LST values were averaged at the pixel level for the dates under consideration, resulting in an urban LST map that represents a summer period.

4. Methodology

In the first step, the Landsat 9 LST product was obtained from the USGS website. An effective variable database at 1 m spatial resolution, including surface topography characteristics, biophysical properties, and land use, was created. The 1-m effective variables were generated by integrating high-resolution spatial datasets. The DSM was used to derive detailed elevation and surface height information at fine spatial resolution, enabling the extraction of 3D urban structure. Land use maps and Google Earth imagery were used to classify surface types through visual interpretation and GIS-based digitization, allowing the identification of key urban features such as buildings, vegetation, and roads.

All datasets were processed and converted into raster layers with a spatial resolution of 1 m using GIS techniques. The variables were then spatially aligned and standardized to ensure consistency across all input layers prior to aggregation and modeling. Aggregation analysis was applied to create a 30-m effective variables map. The second step involved developing a model to estimate urban LST using a machine learning approach. The training data consist of SULST and effective variables at a spatial resolution of 30 m as predictors. A Random Forest (RF) algorithm was employed as a robust and widely used state-of-the-art machine learning method (Breiman, 2001). RF is particularly suitable for this application due to its ability to model nonlinear relationships and handle complex interactions between urban morphological variables and LST without requiring strict assumptions about data distribution.

The Random Forest model was developed using SULST as the dependent variable and aggregated effective variables at 30-m resolution as predictors. The training dataset was constructed by sampling pixels across the study area, ensuring representation of different land use types and surface conditions. The dataset was randomly divided into training (70%) and testing (30%) subsets. To reduce the impact of spatial autocorrelation, samples were selected to ensure spatial dispersion across the study area, minimizing clustering effects.

After that, the developed model was applied to the 1 m effective variables maps to generate the initial downscaled SULST (DSULST) map (1 m). Afterward, this map was aggregated to 30-m spatial resolution through aggregation analysis. Aggregation analysis was conducted to upscale the 1-m resolution variables to 30-m resolution to match the spatial resolution of Landsat 9 LST data. This was achieved by computing the mean value of all 1-m pixels within each 30-m grid cell. This approach is consistent with the physical interpretation of satellite-derived LST, where each pixel represents an average radiometric temperature of mixed surface components. Therefore, mean aggregation was selected as the most appropriate method to ensure consistency between predictor variables and the target SULST data.

Finally, the residual error map was derived by subtracting the 30-m aggregated map from the initial 1-m DSULST map. Then, this error map was applied to the initial DSULST to generate the final 1-m DSULST map. The residual correction approach assumes that the difference between the aggregated downscaled temperature and the original SULST represents a systematic error that can be redistributed to finer spatial scales. This assumption is commonly adopted in thermal downscaling studies; however, it was not explicitly validated in this study and should be considered as a methodological limitation. The test dataset used for model validation was selected as an independent subset not included in the training phase. Despite this separation, the spatial nature of remote sensing data may introduce residual spatial autocorrelation between training and testing samples. This may result in optimistic estimates of model performance.

Model performance was evaluated using multiple statistical metrics, including RMSE, MAE, NRMSE, Pearson correlation coefficient (r), and index of agreement (d), providing a comprehensive assessment of model accuracy.

5. Results

5.1 Model Validation and Evaluation Metrics

The Pearson correlation coefficient (r) between SULST and DSULST is 0.89, indicating a strong linear relationship between SULST and the DSULST (Fig. 2). The root mean square error (RMSE) is 1.15 K and the normalized root mean square error (NRMSE) is 0.095, demonstrating good model performance. Moreover, the comparison shows a small mean absolute error (MAE = 0.56 K), and a high index of agreement (d = 0.95), indicating that the model performs very well (Fig. 2).

The temperature range represented by the DSULST maps is relatively low compared to high-resolution thermal observations reported in previous studies. For instance, Voogt and Oke (1997) reported over 30 K of temperature variability from ~1 m nadir imagery in Vancouver at 10:30 local time. In contrast, Voogt and Oke (1998) reported a temperature range of approximately 10 K in Vancouver for nadir observations averaged across the entire image, which is comparable to the range observed in this study.

These differences can be attributed to several factors. The study area is characterized by limited availability of moist surfaces and the presence of large shaded areas, both of which constrain temperature variability.

Furthermore, it is important to note that the original spatial resolution of Landsat thermal data is 100 m, although it is commonly resampled to 30 m. Consequently, the thermal signal observed in the downscaled data represents spatially averaged radiometric temperatures, meaning that fine-scale thermal variability is not directly measured but instead reconstructed through the downscaling model.

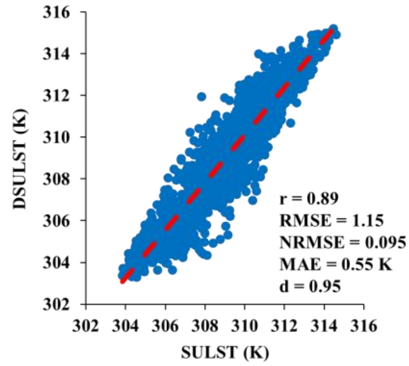

Figure 2. Scatter plot between SULST and DSULST for the study area at 10:30 local time during April-September 2023.

5.2 Spatial Resolution Improvement in Urban LST Mapping

Downscaling SULST from 30-m to 1-m spatial resolution substantially enhances the heterogeneity of urban LST values. The high-resolution DSULST map (1 m) visually highlights clear thermal variations across different surface covers (Fig. 3).

The average SULST derived at the 30-m spatial resolution for the study area was calculated to be 309.1 K, while the corresponding mean value obtained from the DSULST at a finer spatial resolution of 1 m was 308.9 K. The close agreement between these two values indicates a strong consistency between the original coarse-resolution thermal data and the enhanced high-resolution product. This similarity suggests that the downscaling approach has preserved the overall thermal characteristics of the study area while increasing the level of spatial detail.

Despite the minimal difference in mean temperature values, the DSULST data at 1-m resolution provides significantly more detailed insights into the spatial variability of urban surface temperature. In contrast to the aggregated nature of the 30-m data, which tends to smooth out local variations, the high-resolution DSULST map reveals pronounced heterogeneity across the study area. This heterogeneity reflects the influence of diverse urban features, including variations in land cover, building density, surface materials, vegetation distribution, and urban geometry.

The spatial distribution pattern observed in the 1-m DSULST map highlights the presence of localized thermal hotspots and cooler zones that cannot be detected at coarser resolutions. These fine-scale variations are particularly important for understanding the thermal behavior in complex urban environments, where temperature differences can occur over very short distances due to shadow effects, surface properties, and microclimatic conditions.

Overall, the results demonstrate that while the average SULST values at different spatial resolutions remain comparable, the higher-resolution DSULST data provides a more realistic and detailed representation of the urban thermal landscape. Specifically, the DSULST maps exhibit a wider distribution of temperature values, reflecting an increase in the variance at finer spatial scales that is not captured in the coarse-resolution data. In addition, the shape of the temperature distribution is

changed, with a clearer separation of thermal responses associated with different urban surface types. For example, higher temperatures are more distinctly associated with impervious surfaces such as roads and building materials, while lower temperatures correspond to vegetated and shaded areas.
These changes are consistent with the expected thermal behavior of urban materials and surface properties, suggesting that the downscaling process produces physically meaningful spatial patterns. This emphasizes the importance of high-resolution thermal mapping for accurately capturing the spatial heterogeneity of urban LST and for supporting more effective urban climate analysis and planning strategies.

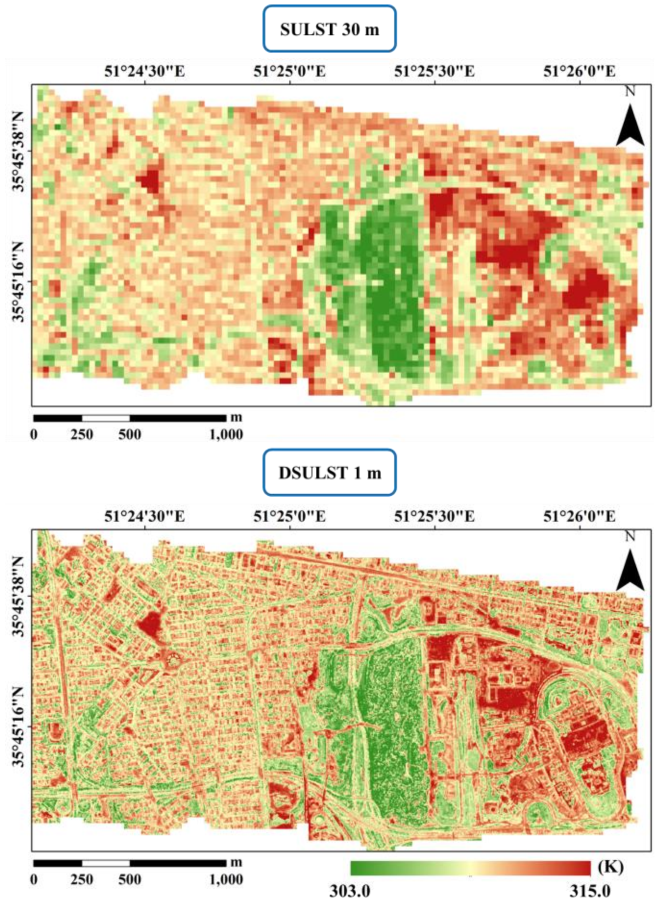

Figure 3. 30-m SULST and corresponding 1-m DSULST maps of the study area at 10:30 local time during April-September 2023.

5.3 Mapping Spatial Comparison of Urban LST with Google Earth Imagery

The maps of SULST (30 m), DSULST (1 m), and Google Earth images for different subregions are shown in Fig. 4. This comparison is intended to provide a qualitative assessment of both accuracy and spatial patterns, as well as to evaluate urban LST variations across different spatial resolutions. Overall, compared to the 30-m SULST maps, the 1-m DSULST maps show substantially more spatial detail. This is primarily because of the higher spatial resolution of the enhanced images, which enables the detection of urban LST variations at finer scales. Consequently, the boundaries between urban features such as buildings, roads, and vegetation are clearly distinguishable in the DSULST maps, while such details are less distinct in the coarser satellite maps. Significant variations in urban LST were observed across different sub-regions of the study area, indicating a highly heterogeneous thermal environment. These spatial differences are mainly driven by several key factors, including land cover type, building density, surface materials, and the orientation of buildings relative to incoming solar radiation. The interaction of these variables plays an important role in shaping the thermal behavior of urban surfaces at fine spatial scales.

For example, areas with dense vegetation cover generally exhibit lower urban LST values compared to regions dominated by built-up structures. Vegetation contributes to surface cooling through evapotranspiration and shading, which reduce heat accumulation and enhance latent heat flux. In contrast, urban areas characterized by high building density and impervious surfaces tend to absorb, store, and re-radiate more heat, resulting in higher surface temperatures.
The type of construction materials used in urban areas also significantly influences thermal patterns. Surfaces such as concrete, asphalt, and cement typically have lower emissivity and higher heat storage capacity than natural surfaces. These surfaces are impervious, which is the main restriction on evaporative cooling, leading to increased sensible heat and decreased latent heat. As a result, such materials contribute to higher urban LST values. Additionally, surface color affects thermal behavior through its control on surface albedo. Darker surfaces, which typically have lower albedo, absorb a greater fraction of incoming solar radiation, leading to increased heat storage. Building orientation relative to the sun is another important factor affecting surface temperature. Structures that receive more direct solar radiation throughout the day tend to have higher surface temperatures, while shaded areas remain cooler. This effect is especially noticeable in dense urban

environments where building geometry creates complex shadow patterns.

Furthermore, the comparison between the high-resolution DSULST maps and Google Earth imagery shows a strong spatial agreement. Areas with dense vegetation consistently correspond to lower urban LST values in both datasets, while regions with concrete and asphalt surfaces exhibit higher temperatures. This consistency confirms the reliability and improved spatial representation of the DSULST data.

Shadow effects are clearly captured in the 1-m resolution DSULST maps, where shaded areas show a noticeable decrease in urban LST. These localized cooling effects are not visible in the coarser 30-m SULST maps, as such maps tend to generalize and smooth out fine-scale variations. This highlights the importance of high-resolution thermal data in accurately capturing micro-scale thermal dynamics and emphasizes its value for detailed urban climate analysis and informed urban planning.

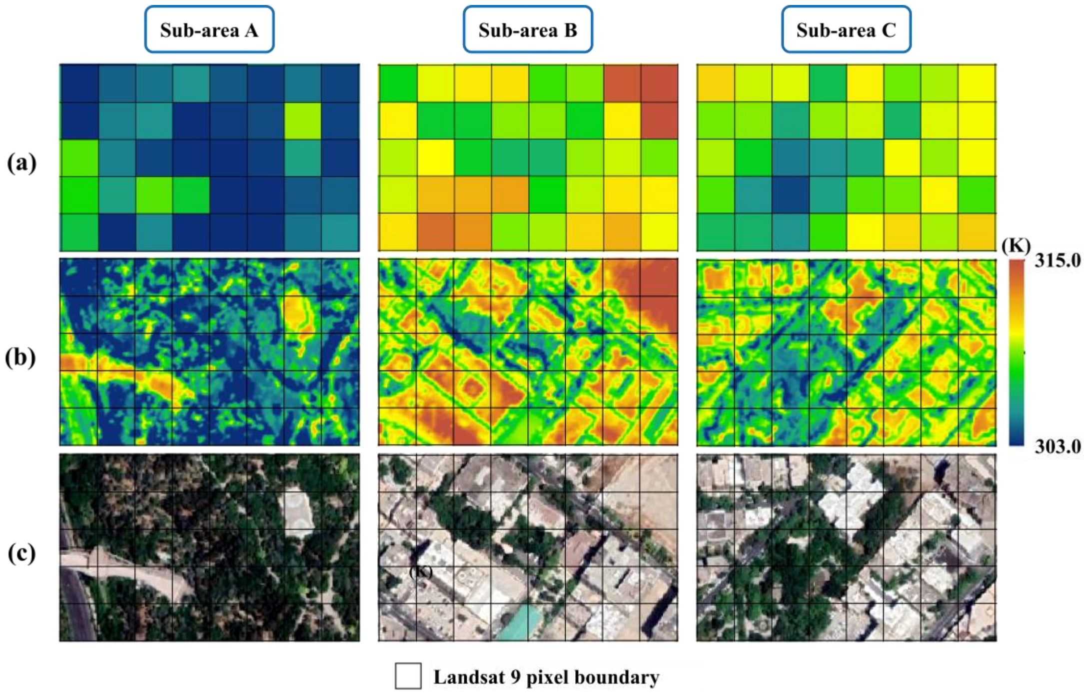

Figure 4. Spatial distributions of (a) 30-m SULST, (b) 1-m DSULST, and (c) corresponding Google Earth images.

6. Conclusion

This study demonstrates how enhancing spatial resolution in urban LST mapping reveals fine-scale thermal variability that is not captured in coarse-resolution data. Comparisons between LST at the initial (SULST) and target (DSULST) resolutions show that significant sub-pixel thermal variability is not captured at the initial resolution, and the boundaries associated with sharp temperature gradients are poorly resolved. The 1-m DSULST maps effectively capture spatial details associated with urban features, such as building roofs, vegetation cover, and ground-level surfaces, while the 30-m SULST maps failed to effectively represent these variations. Consequently, the findings highlight the potential role of high-resolution data in accurately detecting thermal patterns and improving urban heat mitigation strategies. Although the proposed framework shows promising results at the current resolution, its performance requires further evaluation against high-resolution LST data (1 m). Future work should consider validating the method using such fine-scale observations to demonstrate its effectiveness. This study does not explicitly incorporate dynamic atmospheric variables such as wind fields or solar illumination geometry (e.g., sun inclination angle). However, the Landsat 9 images used in this study were all acquired at approximately 10:30 local time, which reduces diurnal variability but does not eliminate variations in solar illumination conditions. Solar zenith and azimuth angles vary throughout the April-September period, which may affect surface energy balance and thermal responses. Due to the absence of independent evaluation data, the sensitivity of the results to these variations was not explicitly assessed. Future work should assess the influence of solar geometry on model performance to better constrain uncertainty.

Furthermore, some indirect effects of solar exposure and shading are implicitly captured through the 3D morphological variables derived from the DSM, which represent urban structure and surface geometry. Nevertheless, the absence of explicit atmospheric and radiative parameters remains a limitation, and future studies should integrate these factors to improve model generalization.

References

Bahi, H., Bounoua, L., Sabri, A., Bannari, A., Malah, A., Rhinane, H., Environment, 2025. A new thermal fusion method to downscale Land Surface Temperature to finer spatial resolution using Sentinel-MSI and Landsat-OLI/TIRS imagery. Remote Sensing Applications: Society and Environment. 37, 101519.

Breiman, L., 2001. Random forests. Machine learning. 45, 5-32.

Firozjaei, M.K., Kiavarz, M., Alavipanah, S.K., 2022a. Impact of surface characteristics and their adjacency effects on urban land surface temperature in different seasonal conditions and latitudes. Building and Environment. 219, 109145.

Firozjaei, M.K., Kiavarz, M., Alavipanah, S.K., 2022b. Satellite-derived land surface temperature spatial sharpening: A comprehensive review on current status and perspectives. European Journal of Remote Sensing. 55, 644-664.

Firozjaei, M.K., Kiavarz, M., Alavipanah, S.K., 2023. An adjacency effect-based approach for accuracy improvement in satellite land surface temperature disaggregation. IEEE Journal of Selected Topics in Applied Earth Observations and Remote Sensing.

Firozjaei, M.K., Mijani, N., Kiavarz, M., Duan, S.-B., Atkinson, P.M., Alavipanah, S.K., 2024. A novel surface energy balance-based approach to land surface temperature downscaling. Remote Sensing of Environment. 305, 114087.

Firozjaei, M.K., Weng, Q., Zhao, C., Kiavarz, M., Lu, L., Alavipanah, S.K., 2020. Surface anthropogenic heat islands in six megacities: An assessment based on a triple-source surface energy balance model. Remote sensing of environment. 242, 111751.

Garuma, G.F., Blanchet, J.-P., Girard, É., Leduc, M., 2018. Urban surface effects on current and future climate. Urban climate. 24, 121-138.

Mashhoodi, B., Stead, D., van Timmeren, A., 2020. Land surface temperature and households’ energy consumption: Who is affected and where? Applied Geography. 114, 102125.

Mijani, N., Alavipanah, S.K., Firozjaei, M.K., Arsanjani, J.J., Hamzeh, S., Weng, Q., 2020. Modeling outdoor thermal comfort using satellite imagery: A principle component analysis-based approach. Ecological Indicators. 117, 106555.

Nuñez, Y., Hoyos, N., Arellana, J., 2023. High land surface temperatures (LSTs) disproportionately affect vulnerable socioeconomic groups in Barranquilla, Colombia. Urban Climate. 52, 101757.

Tahooni, A., Kakroodi, A.A., Mansourian, H., 2025. High-Resolution Urban LST Downscaling via Machine Learning and SHAP: A Case Study in a Rapidly Urbanizing Semi-Arid Region. Sustainable Cities and Society. 106897.

Tanoori, G., Soltani, A., Modiri, A., 2024. Machine learning for urban heat island (UHI) analysis: Predicting land surface temperature (LST) in urban environments. Urban Climate. 55, 101962.

Voogt, J.A., Oke, T., 1998. Effects of urban surface geometry on remotely-sensed surface temperature. International Journal of Remote Sensing. 19, 895-920.

Voogt, J.A., Oke, T.R., 1997. Complete urban surface temperatures. Journal of applied meteorology. 36, 1117-1132.

Voogt, J.A., Oke, T.R., 2003. Thermal remote sensing of urban climates. Remote sensing of environment. 86, 370-384.